Fuel 325 (2022) 124909

Contents lists available at ScienceDirect

Fuel

journal homepage: www.elsevier.com/locate/fuel

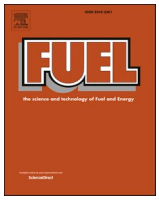

Full Length Article

Effect of active ignition on the end-gas autoignition with detonation combustion in confined space

Lijia Zhong [1], Xiaojun Zhang [1], Lei Zhou [*], Haiqiao Wei

State Key Laboratory of Engines, Tianjin University, Tianjin 300072, China

ARTICLE INFO

Keywords:
End-gas autoignition
Detonation
Pressure oscillation
Confined space

ABSTRACT

In spark-ignition engines, the presence of knock significantly prevents the engines from further improving thermal efficiency. In this work, the effect of active ignition in the end-gas region on the end-gas autoignition with detonation combustion was optically observed in the self-designed constant volume combustion bomb (CVCB-TJU). The different combustion modes together with pressure oscillation were presented. The results indicate that advancing the ignition timing of the end-gas spark can reduce the pressure oscillation intensity and even suppress the occurrence of autoignition. In addition, the present work observed a statistically positive relationship between unburned mass fraction (UMF) and detonation intensity for the knock induced by developing detonation. The underlying influencing mechanism of end-gas ignition on auto-ignition was presented. The end-gas ignition influences the occurrence and intensity of detonation and pressure oscillation by two means: 1) reducing the UMF burned by autoignition, 2) influencing the flame acceleration, thereby reducing the flame tip velocity, and the subsequent shock intensity. Furthermore, the burned mass fraction (BMF) consumed by end-gas flame when jet flames emerge is applied to substitute the ignition timing when measuring its influence at different oxygen concentrations of 29% and 33%. It is found there exists a critical BMF above which the auto-ignition would be suppressed. And this critical value increases with increased oxygen concentration.

1. Introduction

Motivated by the increasingly severe problem of the greenhouse effect and present efforts to mitigate global warming, engines using clean energy are recently attracting more and more attention [1–3]. Among them, hydrogen is extensively investigated due to its potential in realizing carbon-neutral power generation. Compared to traditional spark ignition (SI) engines, the usage of hydrogen facilitates the development of an engine that meet all current emissions standards and regulations with less cost in the after-treatment devices. However, as the acknowledged barrier of spark ignition engine developments, knock significantly prevents the application of hydrogen on SI engines [4] from further improving the thermal efficiency.

An acknowledged theory account for the knock phenomenon is the end-gas auto-ignition mechanism. Before the main flame arrives, the induction time first expires in some hot spots where reactivity gradients exist in a manner described by Zeldovich's theory [5]. The local auto-ignition soon couples with pressure waves induced by heat release, leading to the formation of developing detonation. Quantitative observations [4,6,7] have been conducted to investigate the auto-ignition event and subsequent pressure wave development. For example, Yu and Chen [6] studied the end-gas autoignition (AI) of stoichiometric H_2/air mixture by 1D simulations. In their results, three modes of end-gas combustion were identified. Terashima et al. [7] pointed out that the pressure wave generated by the force ignition and its reflection at the end wall resulted in the formation of hot spots that trigger the autoignition and detonation developments. Oran and her coworkers [8,9] conducted a series of numerical simulations focusing on the interaction of flame, shock wave, wall, and boundary layers. Those works demonstrated the fundamental mechanism of the occurrence of auto-ignition and detonation development. However, there is limited experimental research on the combustion mode transition. Our previous works [10–12] carried out intensive experiments on the self-developed constant-volume combustion bomb (CVCB-TJU) to explore the effect of equivalence ratio, oxygen concentration, and flame velocity on the combustion mode transition. Six different combustion modes, especially the end-gas autoignition and detonation developments were observed. However, the flame propagation and combustion mode with ignition at

* Corresponding author at: 92 Weijin Road, Nankai District, Tianjin, China.
E-mail address: lei.zhou@tju.edu.cn (L. Zhou).
[1] These authors contribute equally to the paper and should be regarded as Co-first author.

https://doi.org/10.1016/j.fuel.2022.124909
Received 22 April 2022; Received in revised form 23 May 2022; Accepted 12 June 2022
Available online 18 June 2022

the end wall is not investigated.

There exist two contradictory opinions on whether knock intensity decreases or increases with the burned mass fraction (BMF) [13–15]. Robert et al. [13] observed an increased knock intensity with decreased BMF, while Kagan and his coworkers [14,15] demonstrated that the knock intensity decreases with decreased BMF. Chen et al. [16] pointed out that both trends could appear depending on the value of the unburned mass fraction (UMF). Note that there is a lack of experimental observations regarding this topic. They also found that a fast enough flame propagation can prevent the occurrence of knock. Extensive efforts had been put into the effects of elevating flame propagation speed to suppress knock in the last decade, which can be generally put into three categories: 1) addition of fuels that have high flame speed; 2) high turbulence flow inside the cylinder; 3) increasing the initial area of flame or reducing flame propagation distance. For instance, Heywood et al. [17] investigate the effect of hydrogen addition on knocking combustion based on a gasoline engine and observed a decreased knock tendency induced by the elevated flame speed. Taiga et al. [18] found a strong relationship between the knock characteristics and in-cylinder intensity, and knock can be suppressed with the increase of turbulence intensity and flame speed. As for the multi-ignitions, the dual-spark system is an easy way to improve combustion speed. Ismaile et al. [19] found that multi-point ignition can ameliorate the in-cylinder combustion process. The CFD model established by Ji et al. [20] suggested that the secondary spark should be kept in line up with the leading spark to achieve the best combustion efficiency. The above investigations provided some understanding of flame propagations in dual-spark systems, however, most of them focused on its effect on elevating flame propagation speed and improving combustion or emission characteristics. In addition, the mechanism of end-gas autoignition with detonation suppression originating from secondary ignition is rare, and further works are supposed to be done, in particular the optical experiment.

Therefore, the present work aims to experimentally reveal the mechanism of end-gas flame suppressing detonation development and observe the combustion mode transition of the end-gas autoignition with detonation combustion by considering an active ignition in the end-gas region for premixed hydrogen-oxygen-nitrogen mixture. The different combustion modes together with pressure oscillation were presented. Additionally, maximum pressures under different ignition timings and oxygen concentrations were considered to present the effect of the unburned mass fraction on detonation occurrence in the end-gas region. Overall, the present work aims to explore the fundamental mechanism of knock suppression by the end-gas active ignition.

This paper is organized as follows: the experimental setup and conditions are briefly discussed in Section 2; the whole evolution of flame propagation and pressure oscillation are presented in Section 3.1; the different combustion modes are summarized in Section 3.2; and finally, the main conclusions from this work are drawn in the last section.

2. Experimental apparatus and procedure

2.1. Experimental apparatus

A self-developed constant volume combustion bomb (CVCB-TJU) was employed in the present study, as shown in Fig. 1. The apparatus is composed of a combustion chamber, intake and exhaust system, heating system, ignition system, perforated plate, time synchronization system, and image acquisition system. The combustion chamber is 100 mm in diameter and 230 mm in length. Due to the existence of optical glasses, the combustion chamber is not a typical cylinder. The total volume of the combustion chamber is 2.32 L. A perforated plate was mounted in the middle of the combustion chamber to accelerate flame propagation and consequently promote the end-gas autoignition. The perforated plate has a porosity of 12% and a diameter of 5 mm. The overall flame propagation, shock formation, and end-gas autoignition were captured by high-speed Schlieren photography. In the present work, a high-speed color camera (Photron SA-Z) adopted with a 105-mm lens (AF Micro Nikkor 1: 2.8 D) was used to capture the flame propagation at 70,000 frames per second with 768 × 352 pixels. The exposure time is 1/200,000 s. Before experiments, the combustion chamber was heated to 363 K to prevent combustion products from liquefaction. More details of the experimental apparatus can be found in our previous works [10–12].

2.2. Experimental procedure

In the present work, premixed hydrogen-oxygen-nitrogen mixture with a unity equivalence ratio was employed. In addition, the initial oxygen concentrations of 29% and 33% were utilized in this work to elevate the reactivity of mixtures. The oxygen concentration of 29% was selected as it ensures the occurrence of detonation, and 33% was further conducted to investigate the effect of end-gas ignition under different flame speeds. In the present work, the masses of oxygen and hydrogen were kept constant to achieve a constant energy density. The masses of

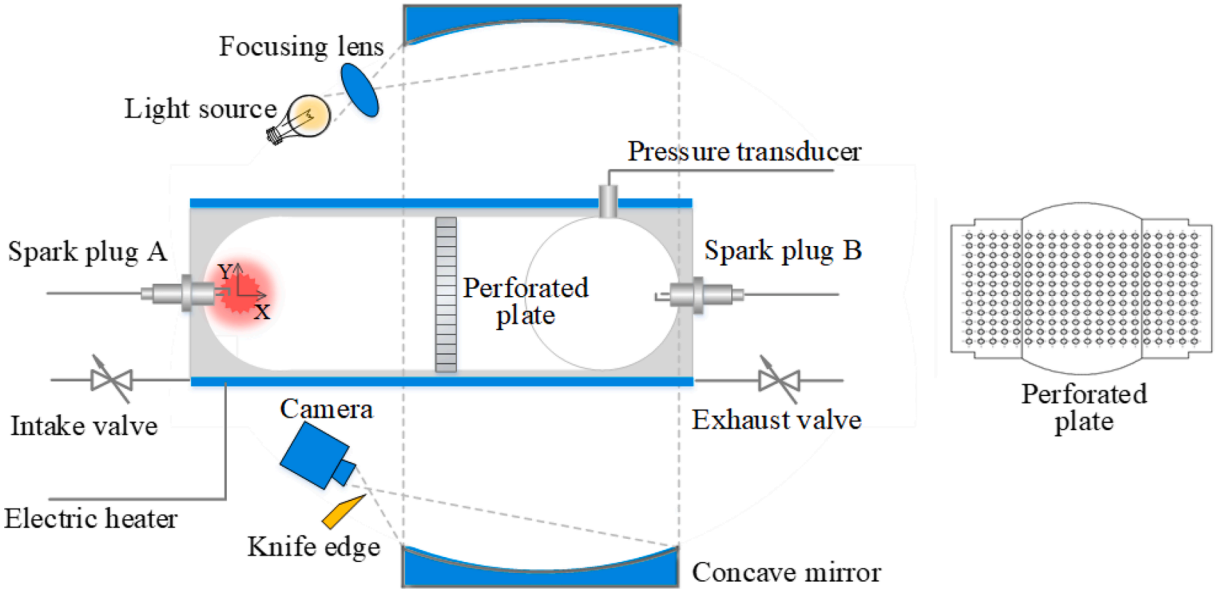

Fig. 1. Schematic of the experimental setup.

oxygen and hydrogen were calculated based on stoichiometric hydrogen/air (21%) mixture at an initial pressure of 3 bar. Then the mass of nitrogen was changed to realize different oxygen concentrations, according to Eq. (1). Therefore, the initial pressure of 29% and 33% conditions were 2.4 bar and 2.2 bar, respectively. The initial temperature is 363 K. Note that the present two oxygen concentrations ensure the occurrence of end-gas auto-ignition and detonation development according to our previous work [12]. In the present work, an extra spark was installed in the middle of the end-wall. The extra spark ignited the end-gas with a delay of 2 ms, 1.5 ms, and 1 ms, respectively. The experimental conditions are listed in Table 1.

$$\text{Oxygen concentration} = \frac{n_{O_2}}{n_{O_2} + n_{N_2}} \tag{1}$$

2.3. Definitions

In the present work, the flame tip velocity (absolute velocity) was used to characterize the flame propagation. It was defined as the time derivation of the flame tip positions in the laboratory frame, which indicate how rapidly the leading edge would traverse a certain distance. Note that the flame tip velocity is not the actual burning velocity, but a superposition of the burning velocity and flow velocity. However, this velocity was extensively used in investigations on flame acceleration and DDTs [21–24]. In addition, in our previous work [25], it was found that flame propagation velocity and subsequent shock intensity dominate the end-gas autoignition and detonation development.

$$Flametipvelocity = \frac{D_{i+1} - D_i}{T_{i+1} - T_i} \tag{2}$$

where D_i represents the distance from the tip to the ignition point at time T_i.

To evaluate the relationship between pressure oscillation and UMF consumed by AI, the UMF is required to be estimated. In the present work, we assumed the end-gas first experience an isentropic compression by the shock wave. Then the density of end-gas is further increased behind the shock. The temperature after the isentropic compression can be estimated as:

$$T_2 = T_1 \left(\frac{P_1}{P_2}\right)^{\frac{1-\gamma}{\gamma}} \tag{3}$$

Table 1
Experimental conditions.

Oxygen concentration	Initial Pressure	Ignition modes	Combustion modes
29%	**2.4 bar**	Single ignition	Autoignition and detonation
		End-gas spark with a delay of 2.0 ms (Delay 2.0 ms)	Autoignition and detonation
		End-gas spark with a delay of 1.5 ms (Delay 1.5 ms)	Autoignition and detonation
		End-gas spark with a delay of 1.0 ms (Delay 1.0 ms)	**Normal combustion**
33%	**2.2 bar**	End-gas spark with a delay of 1.4 ms	Autoignition and detonation
		End-gas spark with a delay of 1.2 ms	Autoignition and detonation
		End-gas spark with a delay of 1.0 ms	Autoignition and detonation
		End-gas spark with a delay of 0.8 ms	**Normal combustion**
		End-gas spark with a delay of 0.5 ms	**Normal combustion**

with the density of mixture calculated by:

$$\rho_1 = \frac{P_1 M}{R T_1} \tag{4}$$

$$\rho_2 = \frac{P_2 M}{R T_2} \tag{5}$$

Then, the pressure and density behind the shock can be calculated by:

$$\frac{P_3}{P_2} = \frac{2\gamma Ma^2}{\gamma + 1} - \frac{\gamma - 1}{\gamma + 1} \tag{6}$$

$$\frac{\rho_3}{\rho_2} = \frac{(\gamma + 1) Ma^2}{(\gamma - 1) Ma^2 + 2} \tag{7}$$

where γ is the specific heat ratio, P, T and ρ are the pressure, temperature, and density of the mixture. M is the molecular weight and R is the gas constant. Ma is the Mach number of the shock wave with respect to the mixture ahead of the shock, and subscribe 1, 2, and 3 denote the initial state, compressed state, and state behind the shock, respectively.

Then the UMF can be estimated by:

$$UMF = \frac{\rho_3 * V_{unburn}}{\rho_1 * V_{total}} \tag{8}$$

3. Results and discussion

3.1. Flame propagation and pressure oscillation

In the present work, five repeated experiments were conducted under each secondary ignition timing. Fig. 2 shows the maximum pressures and combustion modes under different secondary ignition timings. It is observed that with the decrease of ignition delay, the combustion mode shifts from detonation to normal combustion. Note that the detonation mode is discerned from Schlieren images. In addition, both two combustion modes appear in the case with a delay of 1.5 ms. This phenomenon can be explained by the stochastic nature of detonation, which is induced by the multiple stochastic phenomena in the process, including flow instabilities, turbulence, and interactions between shocks, flames and vortices. Furthermore, in the case with a 1 ms ignition delay, the maximum pressure basically remains the same, which verifies the repeatability of the experiments. However, in the cases when detonation occurred, the maximum pressure varies in a wide range under the same condition. This could be explained by two means.

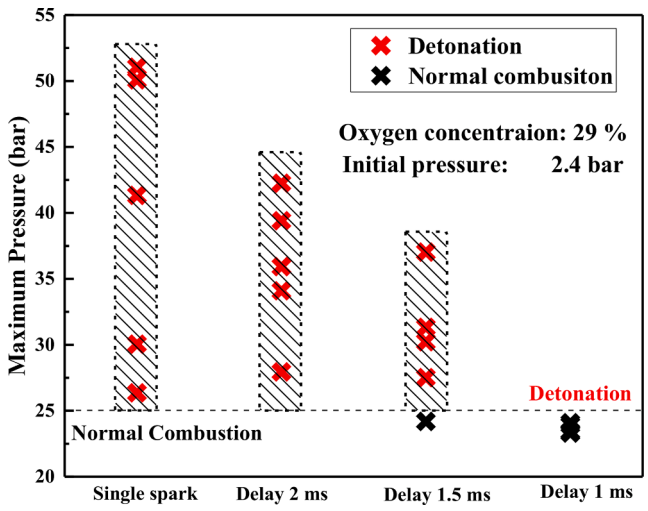

Fig. 2. Evolutions of maximum pressure and combustion mode under different end-gas ignition timings.

On the one hand, limited by the experimental apparatus, the pressure sensor could not ensure capturing the maximum pressure of the detonation. During the experiments, detonation waves formed in the end-gas could have degenerated to shock when they were passing through the pressure sensor. Consequently, the recorded pressure can be influenced by the location of detonation, the distribution of unburned mixture, the UMF, etc. On the other hand, the actual intensity of detonation also shows stochasticity. It is reported by Oran et al. [26] that small fluctuations in the thermal conditions have a significant impact on the detonation.

To demonstrate the flame propagation, end-gas autoignition, and detonation development under different end-gas ignition timings, the case that has max maximum pressure for each secondary ignition timing is selected. Note that though the maximum pressures differ in each test, the flame propagation and flame-shock interaction are basically identical. Fig. 3 displays the flame development and combustion mode transition under different ignition timings of the end-gas spark with an oxygen concentration of 29%. In the single spark condition, the left invisible spark ignites the premixed mixture, generating a right propagating low-speed laminar flame. This flame is deformed into several individual jet flames when it encounters the perforated plate. The flame is significantly accelerated under the delay-burning mechanism [27]. The jet flames soon merge and form a turbulent flame brush. The heat release in the turbulent flame brush generates compression waves ahead

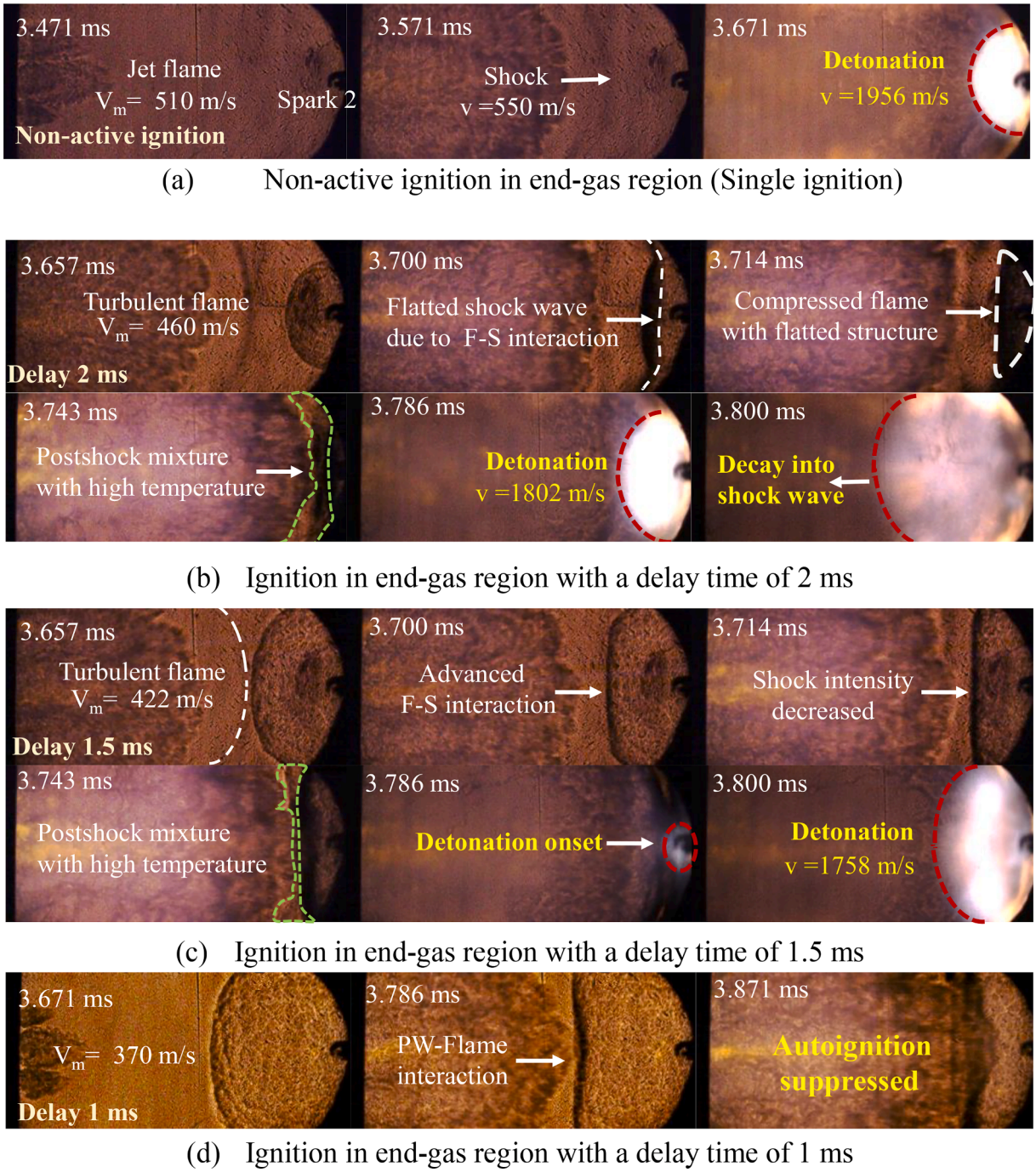

Fig. 3. Sequence photography of combustion processes at different ignition timings of the end-gas spark with an oxygen concentration of 29%. Single ignition denotes the end-gas spark did not work. Delay refers to the working time lag of the end-gas spark compared to the main spark. Vm refers to the mean flame tip velocity from the perforated plate to 60 mm downstream of it.

of it, which are enhanced as they superimpose with each other. Ultimately, a shock wave is formed in front of the turbulent flame at 3.571 ms. The shock finally achieves a velocity of 656 m/s with a Mach number of 1.3 (with respect to the gas ahead of the shock). As the shock wave reaches and is reflected from the end wall, subsequent autoignition is observed due to the decreased ignition delay in the unburned end-gas region. Therefore, a detonation wave with high luminosity is observed propagating towards the left with a velocity of 1956 m/s, which is close to the Chapman-Jouguet velocity (2153 m/s) under the same initial pressure. The detailed physical processes including flame acceleration, shock wave formation and autoignition can be found in our previous work [12,28,29].

In Fig. 3b, a cellular flame induced by thermal-diffusive instability is first observed at the end-gas region, then the jet flame and the subsequent turbulent flame appear. It should be noted that with the introduction of secondary ignition, the appearance of jet flame is delayed, which indicates that the end-gas flame decelerates the propagation of the main flame, even before the formation of turbulent flame. Since the early processes before shock formation are similar to that in the single spark case, we focus on the later development of flame-shock interaction here. At 3.657 ms, the shock wave is formed between the turbulent and end-gas flame, propagating toward the spherical cellular flame. In the next time instance, the shock wave propagates into the burned gas. The shock curvature within the burned gas is slightly flattened due to the flame-shock interaction, while the rest remained unaffected. In addition, the end-gas flame is pushed back due to the flame-shock interaction, with its structure being flattened as well. After that, the shock wave becomes less discernible when it fully enters the burned gas as the density gradient across the shock wave is much smaller in burnt gas [29]. As the turbulent flame propagates, the burned mixture of end-gas flame becomes indistinguishable. At 3.786 ms, the auto-ignition with detonation process takes place on the end wall and it decays into a shock wave. In previous numerical and experimental work [30,31], the flame-shock interaction was found to cause significant deformation in the flame front due to the RM (Richtmyer-Meshkov) instability, which in turn led to the formation of a turbulent flame brush, the creation of hot spots and ultimately, triggered the occurrence of detonation. However, in the present work, the most significant influence of the shock wave on detonation is that it provides a favorable condition for autoignition by significantly reducing the ignition delay.

As the delay decreases to 1.5 ms in Fig. 3**.(c)**, the shock-flame interaction is advanced, as can be seen at 3.657 ms. The physical processes are basically the same with the 2 ms case. However, it is noted that the shock is less discernable here compared to the previous case. Though the speed of the end-gas flame is relatively small, it generates backward-propagating pressure waves ahead flame front. The backward propagating pressure wave reduces the velocity of jet flow. As the jet flow dominates the flame acceleration in the perforated plate, the flame tip velocity of the turbulent flame is significantly reduced due to the secondary ignition. Moreover, the earlier the second ignition, the larger the flow velocity is reduced. Therefore, the flame tip velocity decreases with the advance of the second ignition. Consequently, the shock intensity is further reduced. In this case, the shock only propagates at a Mach number of 1.1. In addition, owing to the increased BMF consumed by the end-gas flame, the unburned mass fraction (UMF) before autoignition decreases. This finding is consistent with previous numerical observations obtained in Ref. [32]. At 3.786 ms, the onset of detonation is observed. As the ignition timing is further advanced to 1 ms, the mean flame tip velocity declines to 370 m/s. In addition, the formation of the shock wave is absent, and only pressure wave-flame interaction is observed. Without the strong shock wave to compress the end burnt gas, the main flame encounters the end-gas flame and consumes all the unburned mixture, thus the autoignition and the subsequent detonation development are suppressed. In the present work, this combustion phenomenon without autoignition and detonation is defined as normal combustion.

The temporal evolution of in-cylinder pressure at different ignition timings is plotted in Fig. 4 to demonstrate the effect of end-gas ignition on detonation intensity. It is found that with the selected cases, the peak pressure and maximum amplitude of pressure oscillation (MAPO) decrease with the advanced ignition timings. In the single spark case, the pressure increases significantly and reaches a maximum value of 5.1 MPa, with a MAPO of 3.2 MPa. Then, the peak pressure declines to 4.2 Mpa in the case with a 2 ms delay. The peak pressure and MAPO keep decreasing with the advance of secondary ignition until the autoignition is suppressed in the last case. Note that the pressure oscillation in the delay 1 ms case is induced by the back and forth propagation of the pressure wave, rather than autoignition. Combined with Fig. 2 which shows that the mean maximum pressure decrease with the advance of secondary ignition, it can be concluded statistically that the detonation intensity decreases with UMF. For a detonation, both the pressure at the detonation onset and the coupling of shock wave and reaction front influence the intensity of the shock wave. In the present work, with the advance of secondary ignition, the pressure of the unburned mixture (estimated by Eq. (6)) decreases from 7.8 bar in the single ignition case to 4.5 bar in the case with a delay of 1.5 ms. In addition, it is observed that with the advance of secondary ignition, the volume of unburned mass decreases as well. For the detonation induced by a hot spot, the coupling of reaction front and pressure wave generated by it is room-required. With a limited fresh gas, the detonation could not be fully developed. As a consequence, the intensity of detonation reduces as well. Therefore, though the recorded maximum pressure exhibits stochasticity under each condition, a statistical relationship could be observed between the detonation intensity and UMF with the advance of secondary ignition.

The flame tip velocities of the main flame and the end-gas flame are displayed in Fig. 5 to demonstrate the overall propagation. It should be noted that the calculation of flame tip velocity stops when the flame is difficult to distinguish. For each case, the jet flame is accelerated based on the delay-burning mechanism found by Bychkov et al. [27]. As the flame propagates to 50 mm downstream of the perforated plate, the combustion upstream of the plate is finished, therefore the flame decelerates as a result of the momentum transfer between the flame and surrounding mixtures. At about 80 mm downstream of the perforated plate, the flame tip velocity is increased again. This is because the formation of shock elevates the local temperature in front of the flame.

The highest flame tip velocity in the single ignition case is approximately 600 m/s. As mentioned above, the flame tip velocity of the main flame decreases with the advance of secondary ignition. In the present work, the maximum flame tip velocity of the turbulent flame reduces from 600 m/s to 423 m/s, and in the 1 ms delay case, the autoignition and detonation are suppressed as a result of the low flame tip velocity. Note that for the actual burning velocity, it is expected the actual burning velocity of the first flame should increase due to the RM instability induced by flame-pressure wave interaction. However, the effect of the second ignition on flow velocity is more pronounced, therefore the flame tip velocity of the first flame which is a superposition of burning velocity and flow velocity decreases.

For the end-gas flame, it should be noted that the pressures at the ignition timing of the second spark are 2.98 bar, 2.60 bar, and 2.45 bar for the 2 ms delay, 1.5 ms delay, and 1 ms delay cases, respectively. Theoretically, the second flame should propagate at a lower speed with the increased pressure at spark timing. However, it is observed from Fig. 5 that the difference between flame tip velocities of the second flames is very small in different secondary ignition timings. This is because the end-gas is elevated to a higher temperature in the later ignition cases, which offsets the influence of higher pressure. Due to the strong flame-shock interaction, the end-gas flame soon attains a velocity significantly faster than the original one, yet in a reverse direction.

In summary, the ignition at the end-gas region suppresses the detonation through two aspects. On the one hand, it consumes the end-gas mixture to reduce UMF consumed by autoignition, thereby decreasing

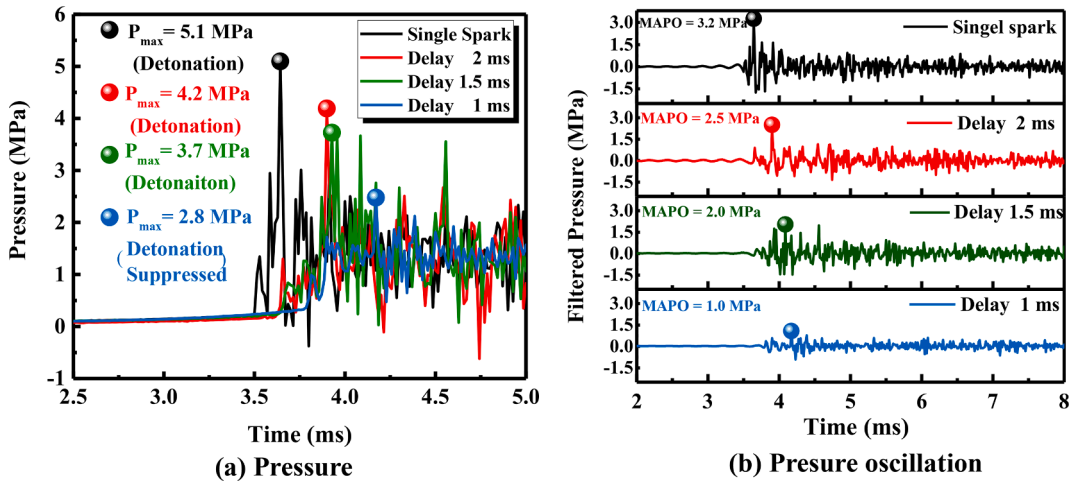

Fig. 4. Evolution of in-cylinder pressure and pressure oscillation at different ignition timings of end-gas spark with an oxygen concentration of 29%. The pressure oscillation is obtained by filtering the pressure with a 4 kHz high pass FFT filter.

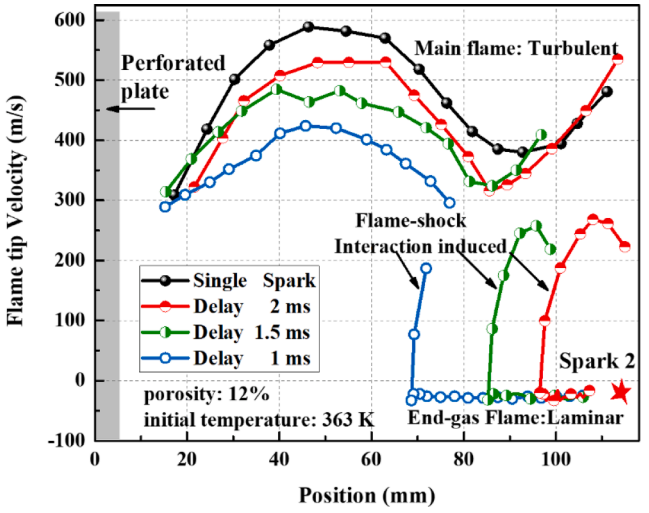

Fig. 5. Tip velocities of the turbulent flame and the end-gas flame as a function of flame tip position under different ignition timings. The uncertainties of the velocities are 10.5 m/s and 1.3 m/s for the main (first) flame and end-gas flame, respectively.

the intensity and possibility of end-gas autoignition. On the other hand, it reduces the flame tip velocity by influencing the flame acceleration of the first flame, thereby decreasing the intensity of the shock wave. Consequently, the detonation is reduced in intensity or even suppressed when the shock is weak enough.

3.2. Effect of oxygen concentration

In practical engines, the high thermodynamic conditions at the top dead center result in an elevated flame speed. In addition, the difference in EGR and operation conditions could lead to variation in flame speed. Therefore, the oxygen concentration of 33% is further conducted to investigate the effect of end-gas ignition timing on autoignition under different flame speeds. Note that the oxygen concentration has a major influence on flame speed but its effect on ignition delay is minor [12]. It turned out that the physical phenomena are the same with cases in 29% concentration, thus the results are not repeated here. However, some interesting results are worthy to share. To normalize the effect of ignition timing of end-gas under different oxygen concentrations and subsequently the varied flame speed, the BMF consumed by end-gas flame when jet flames emerge is used.

Fig. 6 presents the maximum pressures under different secondary ignition timings as a function of BMF consumed by end-gas flame. The practical delay timing of the end-gas spark and the UMF burned by AI are marked near each spot. As explained above, the mean maximum pressure has a negative relationship with the BMF consumed by the end-gas flame for a single oxygen concentration. In detonation cases, the BMF controls the pressure oscillation intensity by reducing the unburned mass fraction consumed by AI. While in autoignition suppressed cases, the maximum pressure changes due to the variation in shock intensity. With the increase of BMF, the combustion mode transforms from developing detonation into normal combustion, indicating that the autoignition and detonation are suppressed at higher BMF conditions. Therefore, the diagram for each oxygen concentration could be separated into two regions based on whether detonation occurred, namely the developing detonation region and the autoignition suppressed region. The right boundary of the detonation region (denoted by blue or orange shaded squares) indicates the critical BMF value, above which the autoignition process will be suppressed. It is found that at a higher

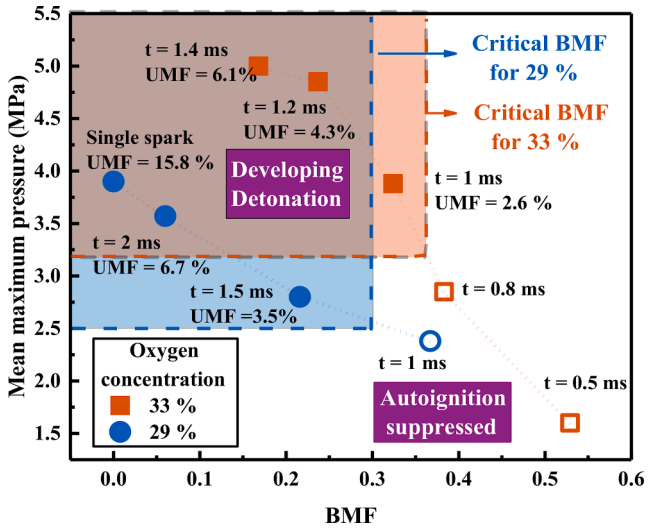

Fig. 6. Maximum pressure under different secondary ignition timings and oxygen concentrations. The horizontal coordinate is defined as the burned mass fraction by end-gas flame when jet flames emerge. The solid samples indicate the occurrence of autoignition while the open samples represent that autoignition and detonation development are suppressed.

oxygen concentration rate, the critical BMF is higher. This could be attributed to the higher flame tip velocities at higher oxygen concentrations [12]. With the higher flame propagation velocity, an earlier and stronger shock wave could be formed, which gives the post-shock unburned mixture a higher temperature and has a stronger capacity to compress the burned end-gas. Consequently, the higher oxygen concentration of 33% can endure more suppression effect of end-gas flame compared to 29%.

In most practical engines, EGR is adopted to reduce the knock occurrence. This is because the EGR dilution reduces the reactivity of fuels. However, in the present work, we aim to investigate the effect of secondary ignition in the end-gas on autoignition and detonation development. Therefore, the effect of EGR dilution is not investigated. But we are glad to give our rough conjecture on what would happen if the mixture were diluted. In general, the most significant influence of EGR dilution is its effect on mixture reactivity. As pointed out in our previous work [25], the diluent acted as an inhibitor for the chemical reaction and moderated the flame acceleration, and thus, restrained the end-gas autoignition and detonation intensity. Consequently, the oxygen concentration to ensure end-gas autoignition and detonation development could be higher. On the other hand, at the same oxygen concentration, the secondary ignition will still take its role in suppressing autoignition and detonation development. In addition, the intensity of detonation will still decrease with the advance of secondary ignition. However, the critical BMF to suppress knock will be reduced due to the decreased reactivity.

4. Conclusions

In the present work, the effect of active ignition at the end-gas region on end-gas autoignition and detonation development was investigated on the self-developed CVCB. The hydrogen/oxygen/nitrogen mixtures with oxygen concentrations of 29% and 33% were applied. The overall flame propagation, shock formation, pressure oscillation, and detonation development under different ignition timings of end-gas spark were observed. It is found that a sufficiently earlier end-gas ignition can even suppress the occurrence of auto-ignition and detonation development. The present work also observed a statistically positive relationship between UMF burned by autoignition and the detonation intensity. The end-gas ignition influences the autoignition development by reducing the UMF burned by autoignition on the one hand, on the other hand, it reduces the shock intensity by reducing the flame tip velocity. The mass fraction consumed by end-gas flame when jet flame emerges is applied to normalize the influence of ignition delay of end-gas spark. It is found that there exists a critical BMF value, above which the autoignition and detonation development will be suppressed. Due to the faster flame propagation in higher oxygen concentration conditions, this critical value increases when the oxygen concentration increases from 29% to 33%.

CRediT authorship contribution statement

Lijia Zhong: Writing – original draft, Data curation, Investigation, Formal analysis. **Xiaojun Zhang:** Methodology, Visualization, Writing – review & editing, Formal analysis. **Lei Zhou:** Conceptualization, Methodology, Writing – review & editing. **Haiqiao Wei:** Supervision, Funding acquisition.

Declaration of Competing Interest

The authors declare that they have no known competing financial interests or personal relationships that could have appeared to influence the work reported in this paper.

Acknowledgments

This work was supported by the Tianjin Natural Science Foundation (Grant No. 20JCYBJC01110) and the National Science Fund for Distinguished Young Scholars (Grant No. 51825603).

References

[1] Luo Q-h, Sun B-G. Inducing factors and frequency of combustion knock in hydrogen internal combustion engines. Int J Hydrogen Energy 2016;41(36):16296–305.
[2] Liu J, Dumitrescu CE. Flame development analysis in a diesel optical engine converted to spark ignition natural gas operation. Appl Energy 2018;230:1205–17.
[3] Dimitriou P, Javaid R. A review of ammonia as a compression ignition engine fuel. Int J Hydrogen Energy 2020;45(11):7098–118.
[4] Levinsky H. Why can't we just burn hydrogen? Challenges when changing fuels in an existing infrastructure. Prog Energ Combust 2021;84:100907.
[5] Zeldovich YB. Regime classification of an exothermic reaction with nonuniform initial conditions. Combust Flame 1980;39(2):211–4.
[6] Yu H, Chen Z. End-gas autoignition and detonation development in a closed chamber. Combust Flame 2015;162(11):4102–11.
[7] Terashima H, Koshi M. Mechanisms of strong pressure wave generation in end-gas autoignition during knocking combustion. Combust Flame 2015;162(5):1944–56.
[8] Gamezo VN, Khokhlov AM, Oran ES. Effects of wakes on shock-flame interactions and deflagration-to-detonation transition. Proc Combust Inst 2002;29(2):2803–8.
[9] Gamezo VN, Khokhlov AM, Oran ES. The influence of shock bifurcations on shock-flame interactions and DDT. Combust Flame 2001;126(4):1810–26.
[10] Zhou L, Zhong L, Zhao J, Gao D, Wei H. Flame propagation and combustion modes in end-gas region of confined space. Combust Flame 2018;190:216–23.
[11] Zhou L, Gao D, Zhao J, Wei H, Zhang X, Xu Z, et al. Turbulent flame propagation with pressure oscillation in the end gas region of confined combustion chamber equipped with different perforated plates. Combust Flame 2018;191:453–67.
[12] Zhao J, Zhou L, Zhong L, Zhang X, Pan J, Chen R, et al. Experimental investigation of the stochastic nature of end-gas autoignition with detonation development in confined combustion chamber. Combust Flame 2019;210:324–38.
[13] Robert A, Richard S, Colin O, Poinsot T. LES study of deflagration to detonation mechanisms in a downsized spark ignition engine. Combust Flame 2015;162(7):2788–807.
[14] Kagan LS, Gordon PV, Sivashinsky GI. A minimal model for end-gas autoignition. Combust Theor Model 2012;16(1):1–12.
[15] Kagan L, Sivashinsky G. Hydrodynamic aspects of end-gas autoignition. Proc Combust Inst 2013;34(1):857–63.
[16] Yu H, Qi C, Chen Z. Effects of flame propagation speed and chamber size on end-gas autoignition. Proc Combust Inst 2017;36(3):3533–41.
[17] Gerty MD, Heywood JB. An investigation of gasoline engine knock limited performance and the effects of hydrogen enhancement. SAE Technical Paper 2006.
[18] Hibi T, Kohata T, Tsumori Y, Namiki S, Shima K, Katsumata M, et al. Study on knocking intensity under in-cylinder flow field in SI engines using a rapid compression machine. J Therm Sci Technol 2013;8(3):460–75.
[19] Altın I, Bilgin A. Quasi-dimensional modeling of a fast-burn combustion dual-plug spark-ignition engine with complex combustion chamber geometries. Appl Therm Eng 2015;87:678–87.
[20] Ji C, Shi C, Wang S, Yang J, Su T, Wang D. Effect of dual-spark plug arrangements on ignition and combustion processes of a gasoline rotary engine with hydrogen direct-injection enrichment. Energy Convers Manage 2019;181:372–81.
[21] Oran ES, Gamezo VN. Origins of the deflagration-to-detonation transition in gas-phase combustion. Combust Flame 2007;148(1–2):4–47.
[22] Ciccarelli G, Dorofeev S. Flame acceleration and transition to detonation in ducts. Prog Energy Combust Sci 2008;34(4):499–550.
[23] Kagan L, Liberman M, Sivashinsky G. Detonation initiation by a hot corrugated wall. Proc Combust Inst 2007;31(2):2415–20.
[24] Bradley D, Lawes M, Liu K. Turbulent flame speeds in ducts and the deflagration/detonation transition. Combust Flame 2008;154(1–2):96–108.
[25] Zhao J, Zhou L, Li K, Zhang X, Pan J, Chen R, et al. Effect of diluent gases on end-gas autoignition and combustion modes in a confined space. Combust Flame 2020;222:48–60.
[26] Gamezo VN, Ogawa T, Oran ES. Flame acceleration and DDT in channels with obstacles: Effect of obstacle spacing. Combust Flame 2008;155(1–2):302–15.
[27] Bychkov V, Valiev D, Eriksson L-E. Physical mechanism of ultrafast flame acceleration. Phys Rev Lett 2008;101(16):164501.
[28] Wei H, Zhao J, Zhou L, Gao D, Xu Z. Effects of the equivalence ratio on turbulent flame–shock interactions in a confined space. Combust Flame 2017;186:247–62.
[29] Wei H, Zhao J, Zhang X, Pan J, Hua J, Zhou L. Turbulent flame–shock interaction inducing end-gas autoignition in a confined space. Combust Flame 2019;204:137–41.
[30] Gamezo VN, Khokhlov AM, Oran ESJC, flame. The influence of shock bifurcations on shock-flame interactions and DDT. 2001;126(4):1810-26.
[31] Thomas G, Bambrey R, Brown CJCT, Modelling. Experimental observations of flame acceleration and transition to detonation following shock-flame interaction. 2001;5(4):573–94.
[32] Chen L, Pan J, Liu C, Shu G, Wei H. Effect of rapid combustion on engine performance and knocking characteristics under different spark strategy conditions. Energy 2020;192:116706.